Available online at www.sciencedirect.com

ScienceDirect

Advances in Climate Change Research xxx (xxxx) xxx

www.keaipublishing.com/en/journals/accr/

Rapid mass loss and disappearance of summer-accumulation type hanging glacier

Chun-Hai XU[a,b,*], Zhong-Qin LI[a], Fei-Teng WANG[b], Pu-Yu WANG[a], Jian-Xin MU[a]

[a] *State Key Laboratory of Cryospheric Science/Tien Shan Glaciological Station, Northwest Institute of Eco-Environment and Resources, Chinese Academy of Sciences, Lanzhou 730000, China*

[b] *National Cryosphere Desert Data Center, Northwest Institute of Eco-Environment and Resources, Chinese Academy of Sciences, Lanzhou 730000, China*

Received 19 May 2021; revised 11 August 2021; accepted 8 November 2021

Abstract

Hanging glaciers hold the absolute dominant number in West China and their changes had important influences on local hydrology, sea-level rise and natural hazards (snow/ice avalanches). However, logistic and operational difficulties have resulted in the lack of *in-situ*-measured data, leaving us with poor knowledge of the changing behaviors of this type of glacier. Here, we presented the spatiotemporal pattern of seasonal and annual mass changes of a mid-latitude hanging glacier in the Tien Shan based on repeated terrestrial laser scanning (TLS) surveys during the period 2016−2018. The distributed glacier surface elevation changes exhibited highly spatiotemporal variability, and the winter elevation changes showed slight surface lowering at the upper elevations and weak thickening at the glacier terminus, which was contrary to altitudinal elevation changing patterns at the summer and annual scales. Mass balance processes of the hanging glacier mainly occurred during summer and the winter mass balance was nearly balanced (−0.10 ± 0.15 m w.e.). The glacier exhibited more rapid mass loss than adjacent other morphological glacier and the estimated response time of the glacier to climate change was very short (6−9 years), indicating hanging glaciers will experience rapid wastage and disappearance in the future even with climate change mitigation.

Keywords: Hanging glaciers; Mass balance processes; Glacier disappearance; Tien Shan; Climate change

1. Introduction

The hanging glacier is defined as a glacier that hangs on the hillside and cannot descend to the foot of a mountain (Qin, 2016). This type of glacier is characterized by small size (usually less than 1 km^2) and thin ice thickness and is very sensitive to climate change (Qin, 2016; Margreth et al., 2017). Despite their area is relatively small, the number of hanging and cirque-hanging type glaciers take predominance in absolute number in China (Shi, 2008). Hanging glaciers are even relevant at large scales since their vast number, short response time and snow/ice avalanches (Vincent et al., 2015; Faillettaz et al., 2016). However, the studies concerning hanging glaciers are currently sparse, which resulted in an important knowledge gap concerning the glacier dynamic process and glacier−climate interactions.

Glacier mass balance is the direct and immediate signal of climate change (Zemp et al., 2015; Huss et al., 2021). The *in-situ* measurements (also called the glaciological method) use extensive stakes and snow pits to measure the annual or seasonal glaciological mass balance of individual glaciers. The method can provide high spatiotemporal variability of glacier surface mass balance, which is extremely expensive and time-consuming and often gives low spatial coverage (inaccessible areas, such as crevasses, steep ice, debris cover, etc., often

* Corresponding author. State Key Laboratory of Cryospheric Science, Northwest Institute of Eco-Environment and Resources, Chinese Academy of Sciences, Lanzhou, 730000, China.

E-mail address: xuchunhai@lzb.ac.cn (XU C.-H.).

Peer review under responsibility of National Climate Center (China Meteorological Administration).

https://doi.org/10.1016/j.accre.2021.11.001

Please cite this article as: XU, C.-H., et al., Rapid mass loss and disappearance of summer-accumulation type hanging glacier, Advances in Climate Change Research, https://doi.org/10.1016/j.accre.2021.11.001

exist), all of those have contributed to the small number and heterogeneous spatiotemporal distribution of glaciological mass balance (Hoelzle et al., 2017). From our field investigation, hanging glaciers are usually characterized by very steep slopes and glacier surface is therefore almost inaccessible, which limits the implementation of glaciological measurements. To our knowledge, few studies have reported the mass balance of hanging glaciers in China so far.

By contrast, mass balance can also be measured by differencing multi-temporal digital elevation models (DEMs) via the geodetic method (Zemp et al., 2019). However, the retrievable DEMs derived from the current remote sensed images usually limited the temporal resolution of coarse geodetic mass balance to multi-annual to decadal intervals (Zemp et al., 2019). Most of the available global satellite imageries are outdated and fundamentally flawed, such as the penetration of snow and ice for Shuttle Radar Topography Mission (SRTM) C-band DEM (Paul, 2008). High-precision survey technologies, for instance, real-time kinematic (RTK) global navigation satellite system (GNSS), unmanned aerial vehicle (UAV) and light detection and ranging (LiDAR) can cope with the challenges of traditional imageries and capture local-scale processes of mountain glaciers (Immerzeel et al., 2014; Schumann and Bates, 2018). However, RTK surveys are similar to the glaciological method and only give low spatial coverage. UAV may cover the shortage of RTK surveys, but the limited flight altitude and rapid battery consumption usually reduce the capacity of surveys by aircraft (Fugazza et al., 2018). Three-dimensional (3-D) laser scanning allows the acquisition of dense point clouds and then the creation of high-precision and -resolution DEMs (Joerg et al., 2012; Helfricht et al., 2014; Colucci et al., 2015; Fischer et al., 2016; Klug et al., 2018).

Terrestrial laser scanning (TLS) system can more easily capture glacier changes with high time resolution compared with the high cost of airborne laser scanning (ALS) surveys. Huge terrain undulations and high-altitude massif restrict the flight range since most ALS devices also have limited flight altitude. In addition, the steep terrain of hanging glaciers often leads to the existence of unscanned areas in ALS surveys when the incident angle of laser pulse relative to a glacier surface is too small (Xu et al., 2019). TLS is especially suited for the measurements of annual or seasonal geodetic mass balances of hanging glaciers since the relative large incident angle (steep surface slope of hanging glaciers) and almost the whole glacier surface is visible (glacier size is small) from one scan position (Fischer et al., 2016; López-Moreno et al., 2016). Under this opportunity, the knowledge gap about glacier mass changes of the hanging glacier can be filled.

Up to now, TLS is mainly utilized to monitor valley, cirque glacier, debris-covered and rock glaciers (e.g., Gabbud et al., 2015; Fischer et al., 2016; López-Moreno et al., 2016; Fugazza et al., 2018; Xu et al., 2019; Ulrich et al., 2021). Some of those studies demonstrate that TLS surveys can generate high-quality geodetic mass balances, which are in close agreement with glaciological measurements (Fischer et al., 2016; Xu et al., 2019). New long-range Riegl VZ®-6000 TLS is a well-established tool for measuring snowy and icy terrain even at long distances as the device operates at the wavelengths in the near-infrared band (class 3B laser beams, 1064 nm), which enables high rates of reflection (>80%) (RIEGL, 2014). In this context, Riegl VZ®-6000 TLS was applied, and the main aim of this study is to show the spatiotemporal pattern of seasonal and annual mass changes of a mid-latitude hanging glacier in the Tien Shan, to discuss the possible mechanism of the changing pattern, including snow/ice avalanches, and to deepen our knowledge of the changing behavior for the hanging glacier. Our study will aid to better understand the characteristics of mass changes of hanging glaciers and associated impacts in western China.

2. Study site

The study site is situated in the source of the Urumqi River, Tien Shan (Fig. 1). Here, the investigated glacier (43.102°N, 86.828°E) is a typical northwest-facing hanging glacier (mark in Fig. 1c). The glacier is situated beside Urumqi Glacier No.1 (the straight line distance is about 1.2 km), which is one of the reference glaciers in the World Glacier Monitoring Service (WGMS) with detailed annual and seasonal glaciological mass-balance measurements. According to the latest TLS surveys on 28 August 2018 (Fig. 1b), the hanging glacier had an area of 0.051 km^2 with a mean surface slope of 42.29°, the glacier elevations extended from 3818 to 4055 m a.s.l with a median elevation of 3948 m a.s.l.

Urumqi River is characterized by a continental climate setting, the dynamic action of the Tibetan Plateau influences the westerly circulation in winter and results in a cold climate with scarce precipitation in the river, and the Tibetan Plateau develops into a thermal depression and forms a plateau monsoon in summer, which brings warm and humid air from the Indian Ocean, producing abundant precipitation surrounding the plateau (Xu et al., 2018b). The meteorological records of the nearby Daxigou meteorological station (located about 3 km southeast of the glacier at 3539 m a.s.l.) showed that high air temperature and about 78% of the annual total precipitation with the type of snow, hail and sleet occurred simultaneously during May−August (Yang et al., 1992; Yue et al., 2017). It is widely recognized that air temperature and precipitation of glacierized regions are the main factors controlling glacier mass balance, the aforementioned climatic conditions determine that both strong accumulation and ablation of the hanging glacier occur synchronously in summer, thus we defined the hanging glacier as a summer-accumulation-type glacier (Li et al., 2011). Note that the nearby Urumqi Glacier No.1 is also a typical summer-accumulation-type glacier since it is situated in the same climate setting (Wang et al., 2014; Yue et al., 2017; Hoelzle et al., 2017). Thus our results can be compared with Urumqi Glacier No.1 to investigate the possible discrepancy of different morphological types of glaciers response to climate warming.

3. Data and methods

We performed five scan campaigns by using the Riegl VZ®-6000 to collect TLS data. The instrument was designed by

Please cite this article as: XU, C.-H., et al., Rapid mass loss and disappearance of summer-accumulation type hanging glacier, Advances in Climate Change Research, https://doi.org/10.1016/j.accre.2021.11.001

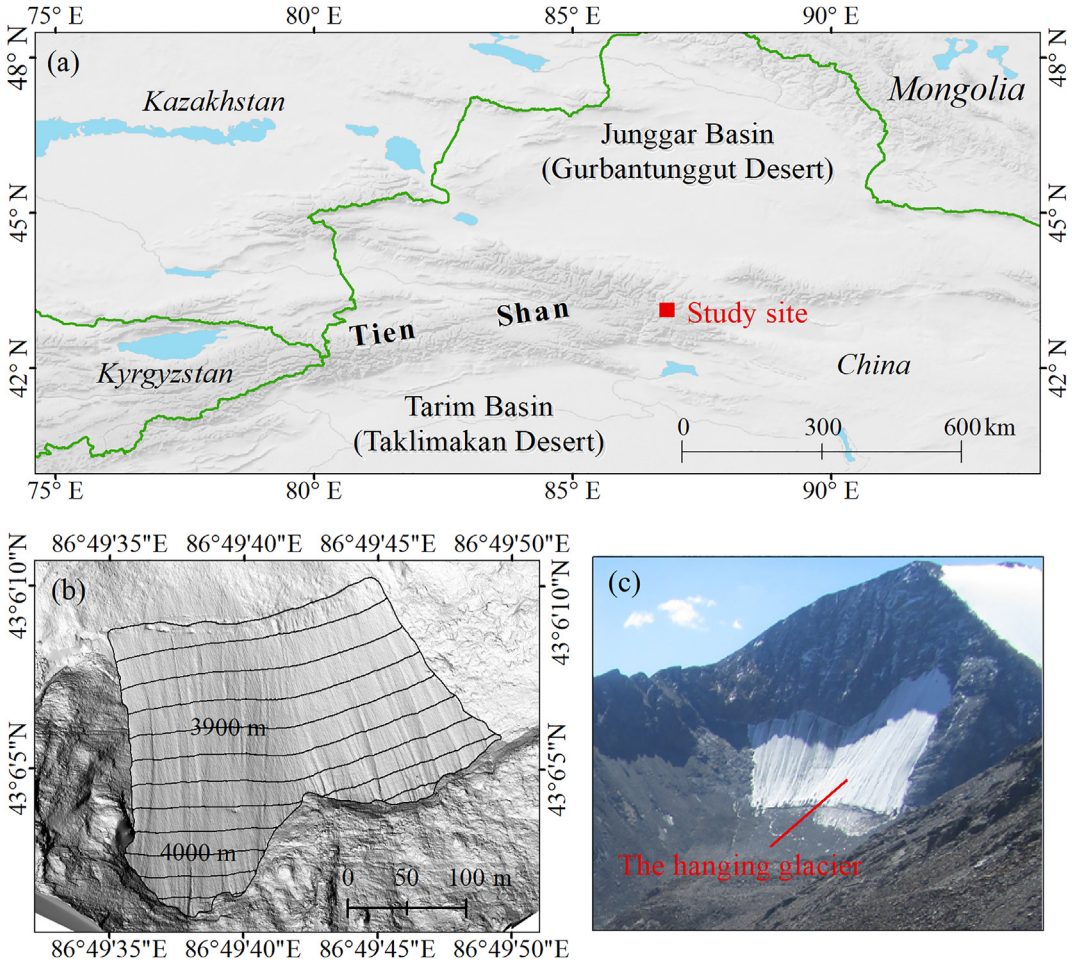

Fig. 1. (a) Location of the hanging glacier in the Chinese Tien Shan, (b) surface terrain (contour in 20 m interval) and glacier boundary of the hanging glacier (black polygon), which were delineated from TLS-derived DEM on 28 August 2018, and (c) the picture of the glacier was taken in September 2018.

Riegl Laser Measurement Systems GmbH (Austria) with a maximum measuring range of 6000 m and ranging precision of 10 mm (RIEGL, 2014). The detailed performances have been described by Gabbud et al. (2015) and Fischer et al. (2016). Here, one scan position was used for the TLS surveys and 3-D coordinate of the scan position was surveyed using Trimble R10 GNSS with the type of static measurement, and the horizontal and vertical accuracy was reported to be about 3 mm + 0.5 ppm and 5 mm + 0.5 ppm, respectively. Point clouds of the scan campaigns were obtained at the beginning and end of the ablation seasons to get summer, winter and annual mass balance according to the long-term glaciological mass balance measurements of Urumqi Glacier No.1 (Liu et al., 1997). Detailed survey parameters are given in Table 1.

We pre-processed the TLS data using RiSCAN PRO® 1.8.1 software and ArcGIS 10.2.2 software, including direct georeferencing, compression, filtering, multi-temporal registration and interpolation. For each scan campaign: we first used the high-precision 3-D coordinate of the scan position to convert the point cloud data from the scanner's own coordinate system into the global coordinate system (in the WGS84 datum with a UTM 45N projection) to complete direct georeferencing, and then point cloud was compressed with an equal space of 0.1 m and noise or non-ground data was filtered out. After these, we configured processed point clouds of the scan campaign on 28 August 2018 as a reference layer to implement multi-temporal registration by using iterative closest point algorithms. Interpolating the processed point cloud generates high-accuracy and -resolution DEMs (0.1 m) after multi-temporal registration. The workflow of point cloud processing is described in detail by Xu et al. (2019).

The geodetic (specific) mass balance (B_{geod}) is calculated based on the multiplication between volume changes (ΔV) a volume-to-mass conversion factor (ρ):

Table 1
Seasonal and annual survey parameters.

Date (yyyy/mm/dd)	Number of points	Scanning range (m^2)	Point density (points m^{-2})	Applied angle increment (°)
2016/05/03	3,557,110	385,100	9.24	0.01
2016/09/01	3,543,966	354,650	9.99	0.01
2017/04/29	3,594,748	397,850	9.04	0.01
2018/08/28	3,581,168	369,900	9.68	0.01

Please cite this article as: XU, C.-H., et al., Rapid mass loss and disappearance of summer-accumulation type hanging glacier, Advances in Climate Change Research, https://doi.org/10.1016/j.accre.2021.11.001

$$B_{\text{geod}} = \frac{\Delta V}{S} \cdot \frac{\rho}{\rho_{\text{water}}} \quad (1)$$

where S denotes the mean glacier area of the two TLS survey times by assuming a linear change (Zemp et al., 2019), ρ_{water} is the density of water. A commonly applied conversion factor of 850 ± 60 kg m^{-3} is used to convert glacier volume changes into geodetic mass balance since the *in-situ* measurements of snow/firn densities of the hanging glacier are lacking (Huss, 2013).

Glacier area is an important parameter for geodetic mass balance estimates according to Eq. (1). Following Abermann et al. (2010). We firstly calculated two shade reliefs on 1 September 2016 and 28 August 2018 (at the end of the ablation season) with an azimuth angle for illumination (300°) based on TLS-derived high-resolution DEMs to show optimal visualization of contrasts in different aspects. Then we delineated the glacier boundary directly by manually digitizing the strongest roughness in the shade reliefs (Fig. 2).

The uncertainty of glacier surface elevation changes ($\sigma_{\overline{\Delta h_{\text{TLS}}}}$) was assessed following Rolstad et al. (2009) based on the geostatistical analysis methods and calculated with

$$\sigma_{\overline{\Delta h_{\text{TLS}}}}^2 = \sigma_{\Delta h_{\text{TLS}}}^2 \cdot \frac{1}{5} \cdot \frac{S_{\text{cor}}}{S} \quad (2)$$

where S_{cor} denotes the correlation area, $\sigma_{\Delta h_{\text{TLS}}}$ denotes the standard deviation of the elevation bias in the non-glacierized stable terrain (Fig. 3) and S equals to S_{cor} since the high-density of the point cloud (Rolstad et al., 2009; Joerg et al., 2012). Then we estimated the uncertainty of geodetic mass balance (σ_{geod}) as:

$$\sigma_{\text{geod}} = \pm\sqrt{(\overline{\Delta h_{\text{TLS}}} \cdot \sigma_\rho)^2 + (\rho \cdot \sigma_{\overline{\Delta h_{\text{TLS}}}})^2} \quad (3)$$

where $\overline{\Delta h_{\text{TLS}}}$ is the average glacier surface elevation changes and σ_ρ is the error of the density conversion (60 kg m^{-3}) (Table 2).

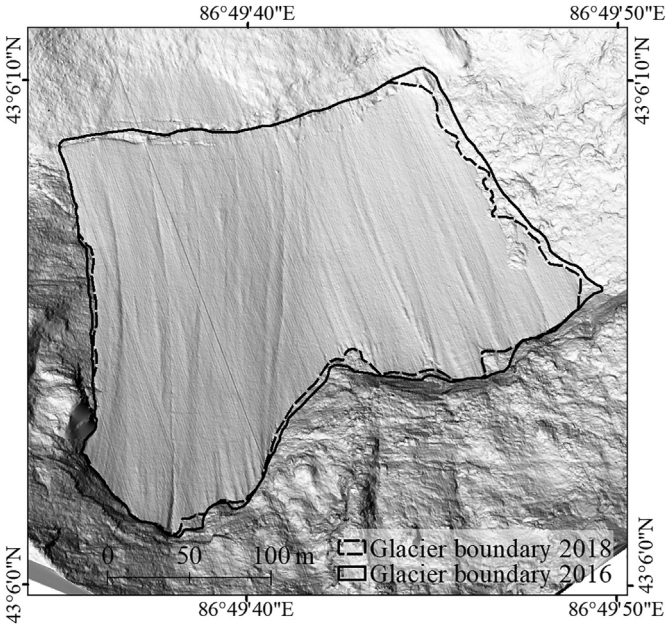

Fig. 2. Creation of the shaded reliefs of the hanging glacier margin according to the TLS-derived DEM (28 August 2018) with the glacier boundary in 2016 and 2018.

Table 2
Error (σ_{MSA}) of Multi-Station Adjustment (MSA), the number of points (n) used for multi-temporal registration of two consecutive scan campaigns, the uncertainty of TLS-derived glacier surface elevation ($\sigma_{\overline{\Delta h_{\text{TLS}}}}$) and corresponding uncertainty of geodetic mass balance (σ_{geod}) were also listed.

Period	σ_{MSA} (m)	Number of points	$\sigma_{\overline{\Delta h_{\text{TLS}}}}$ (m)	σ_{geod} (m w.e.)
2016 summer	0.059	47,314	0.15	0.16
2017 winter	0.084	41,389	0.17	0.15
2016–2018	0.056	59,723	0.06	0.13

4. Results

4.1. Changes in glacier surface elevation and mass balance

The TLS-derived high-resolution DEMs (0.1 m) provided exceptional levels of a detailed glacier surface elevation change and its spatial variability. The spatial patterns in surface elevation changes of the hanging glacier presented a significant difference among summer, winter and annual scales (Fig. 4). Distributed glacier elevation change exhibited pronounced thinning at the lower-elevation parts with the most negative values up to −4.0 to −3.5 m, gradually decreasing with the increase of altitude, and slight thickening was observed at higher elevations with positive values in the range of 0–1 m during the summer months. Elevation change patterns were contrary over the winter mass-balance period and the relatively slight surface lowering occurred at the upper elevations and weak thickening was observed at the glacier terminus, the proportion of surface lowering area was about 59.8% of the whole glacier. At the annual scale, glacier surface lowering occurred across all the elevations and was pronounced at the terminus with 99.4% of the elevation changes falling in the range of −4.0 to −1.0 m. In addition, some stripes of noticeable thinning were observed for all of the three periods, which were probably related to snow/ice avalanches.

Multiplying the spatially distributed glacier surface elevation changes and density conversion factor gives glacier-wide geodetic mass balance. Our results suggested that the summer and annual mass balance were clearly negative with the values of −1.38 ± 0.16 m w.e. and −0.86 ± 0.10 m w.e. per year for summer 2016 and the period 2016–2018, respectively, and the winter mass balance was almost close to zero with a value of −0.10 ± 0.15 m w.e., confirming that the glacier mass–balance processes mainly occurred during the summer

Please cite this article as: XU, C.-H., et al., Rapid mass loss and disappearance of summer-accumulation type hanging glacier, Advances in Climate Change Research, https://doi.org/10.1016/j.accre.2021.11.001

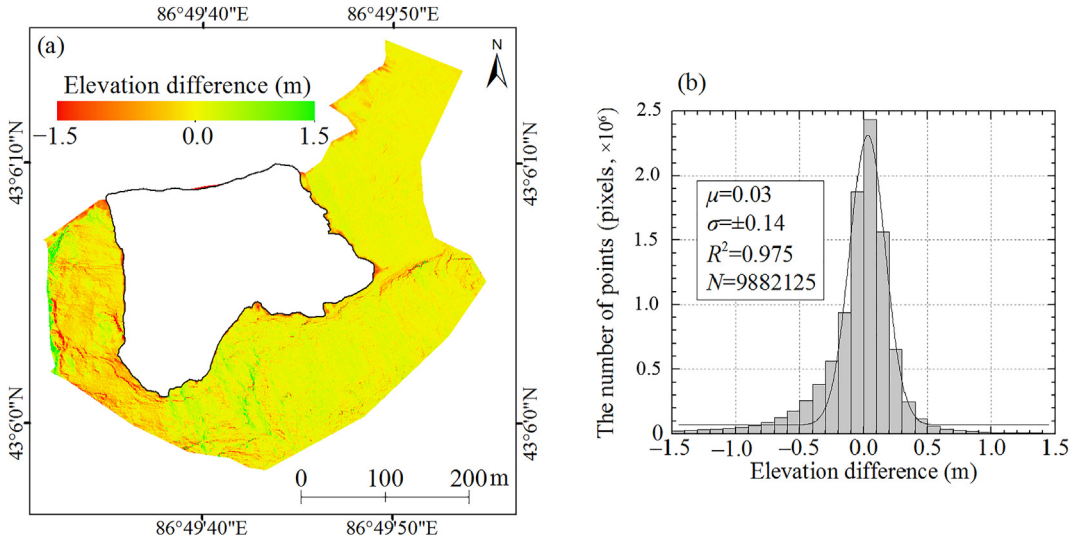

Fig. 3. (a) Spatially distributed elevation changes over stable non-glacier terrain for the two complete mass-balance years (2016−2018), (b) corresponding frequency distribution of these changes over stable terrain (The median (μ), standard deviation (σ), fitting coefficient (R^2) and the number of pixels (N) over the stable non-glacier terrain are given).

months. The magnitude of summer, winter and annual mass balances were consistent with other morphological shapes of glaciers. Thus, the hanging glacier presented a similar response to climate warming and was a valuable indicator.

4.2. Altitudinal distribution of glacier surface elevation changes

The altitudinal elevation changes are the comprehensive result of glacier dynamic processes and mass balance. Therefore, changes in glacier elevation over the altitude can help us understand glacier status between different morphological shapes. Overall, we observed decreasing thinning with altitude at the summer and annual scales, which was a commonly changing pattern and agreed well with the glaciological measurements of other morphological shapes of glaciers (WGMS, 2020). But the altitudinal distribution of elevation changes exhibited an opposite pattern in winter, and reduced slight thickening and increased slight thinning were observed at the terminus and high elevations, respectively, potentially due to the removal of existing snow depositions from the high elevations to glacier terminus since the steep slope of high elevations existed and very poor precipitation was observed by Daxigou meteorological station during winter, which cannot supply large fresh snow for glacier accumulation in the high elevations (Fig. 5a). Specifically, increased annual surface lowering was observed at the glacier terminus and relatively small thinning occurred at the altitude below 3900 m a.s.l., which could be due to remarkable accumulation at the upper-left corner of the glacier during the winter (Fig. 4b), and the thinning then continuously decreased with increasing altitude. Compared with the annual altitudinal elevation changes, summer glacier thinning was more negative in the lower elevations and more positive in the higher glacier parts. The discrepancy of summer and annual altitudinal elevation changes may be related to the climate setting, which determines that both strong accumulation (mainly occurs in high elevations) and ablation (mainly occurs in low elevations) of the hanging glacier mainly take place during the summer months. Additionally, the steep slope at the higher elevations may increase the removal of large snow depositions by avalanches (Fig. 7a), which was confirmed by the observed stripes with notable thinning in Fig. 4c (Xu et al., 2018a). Annual altitudinal elevation changes were therefore more negative at the high-elevation parts than the summer changes. We compared the altitudinal elevation changes in summer 2016 with the TLS-derived corresponding results of Urumqi Glacier No.1, which showed that surface lowering of the hanging glacier was generally larger than Urumqi Glacier No.1, especially for the west branch of Urumqi Glacier No.1 (Fig. 5b). The exception was the glacier terminus, the higher thinning of Urumqi Glacier No.1 was observed at the glacier terminus, which was probably attributed to glacier retreat. This finding suggested that the hanging glacier was more sensitive to climate change compared with other morphological shapes of glaciers in the same local climate setting and thus exhibited more rapid mass loss.

5. Discussion

5.1. Climate and local terrain controls

Air temperature and precipitation are the main climatic factors controlling glacier mass−balance processes (Li et al., 2021). Meteorological records of the Daxigou meteorological station confirmed that more than 70% of the daily mean air temperature was considerably lower than 0 °C and precipitation was also very poor during winter (September to April of the next year). Glacier ablation is directly related to the air temperature (the sum of daily mean air temperatures

Please cite this article as: XU, C.-H., et al., Rapid mass loss and disappearance of summer-accumulation type hanging glacier, Advances in Climate Change Research, https://doi.org/10.1016/j.accre.2021.11.001

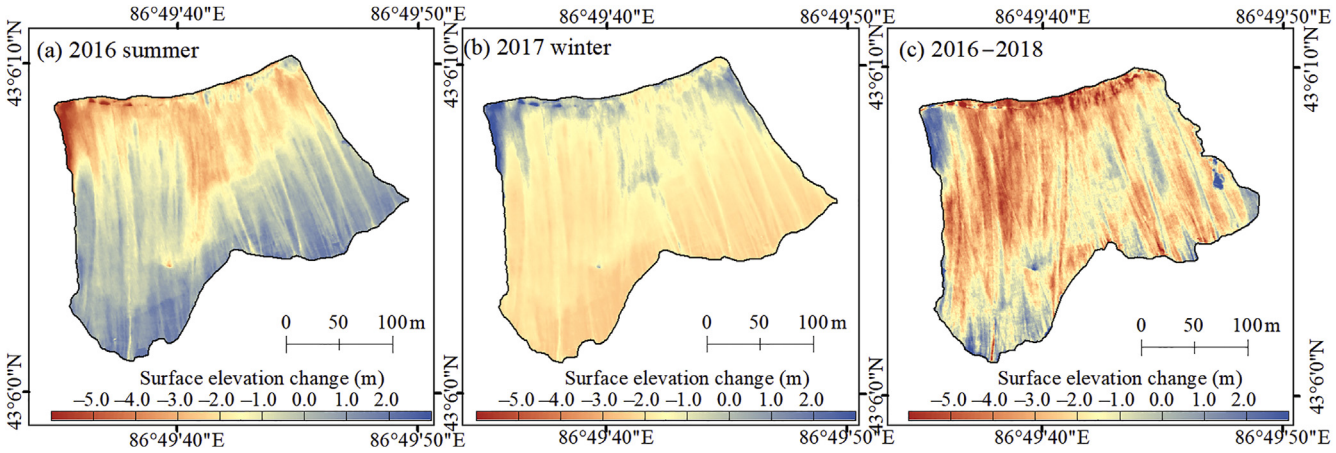

Fig. 4. Spatial distribution of seasonal (a, b) and annual (c) glacier surface elevation changes (The black polygon indicates the TLS-derived glacier outline in the corresponding years).

above 0 °C) and accumulation directly depends on solid precipitation (Qin, 2016). The above-mentioned low air temperature and very poor precipitation would probably result in slight negative mass balances in winter 2017 (Fig. 6). High air temperature (>0 °C) mainly occurred in summer (April to September), which may cause pronounced summer mass loss.

Our results suggested that the hanging glacier exhibited more negative summer mass balance than Urumqi Glacier No.1 (−1.03 m w.e.) and the observed mean annual geodetic mass balance was slightly more negative compared to the direct glaciological value of Urumqi Glacier No.1 (−0.70 m w.e. per year over the two-consecutive mass-balance years (2016−2018)). But the winter mass balance was negative for the hanging glacier and positive for Urumqi Glacier No.1, which may be related to local terrain controls, the steep slope of the hanging glacier surface was detrimental to glacier accumulation. As shown in Fig. 7a, glacier surface slope increased approximately linearly with the increase of altitude, and the mean surface slope of the hanging glacier was 42.37° in 2016, indicating glacier surface presented a slightly decreasing trend over the recent two years and the decrease mainly occurred at the middle-elevation regions. Surface slope of the upper elevations and glacier terminus presented an increasing trend over the two years, which will accelerate the removal of snow depositions and contribute to ongoing glacier mass loss. This may explain glacier thinning was observed even at high elevations. Additionally, glacier surface slope and elevation changes exhibited a significant negative correlation, indicating the steep slope of the glacier surface can increase the removal of snow depositions by avalanches (Fig. 7b).

5.2. Hanging glacier change in future

Several recent studies have found that glaciers in High Mountain Asia will continue to shrink under the background of climate warming or even climate change mitigation since

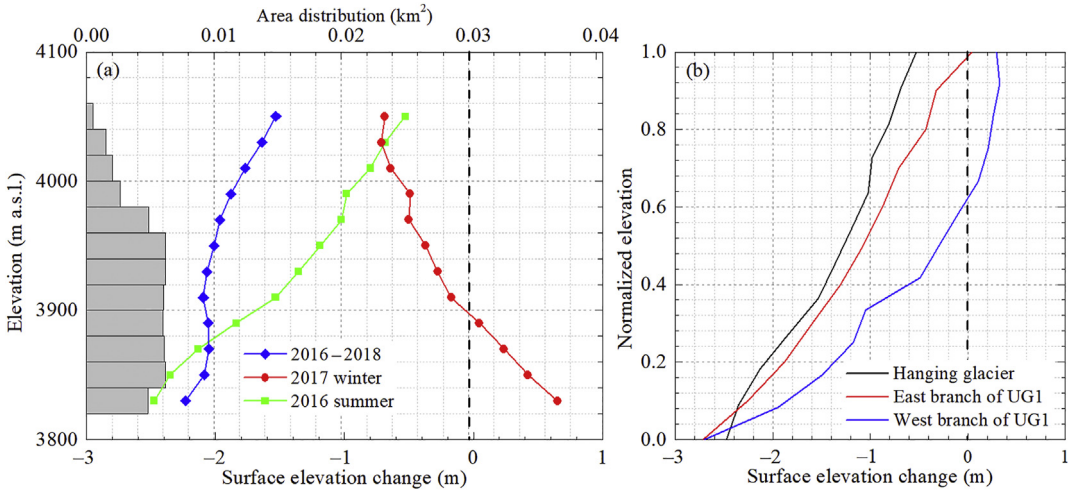

Fig. 5. (a) Altitudinal distribution of glacier surface elevation changes as well as hypsometry of the total glacier area (grey histograms) in 2018, (b) comparison of the altitudinal elevation changes between different morphological shapes of glaciers (UG1-Urumqi Glacier No.1) for summer 2016 versus normalized elevation, which is calculated based upon $(h–h_{min})/(h_{max}–h_{min})$, here h is the mid-value of each elevation band (20-m interval), h_{min} and h_{max} are the maximum and minimum elevation bands, respectively.

Please cite this article as: XU, C.-H., et al., Rapid mass loss and disappearance of summer-accumulation type hanging glacier, Advances in Climate Change Research, https://doi.org/10.1016/j.accre.2021.11.001

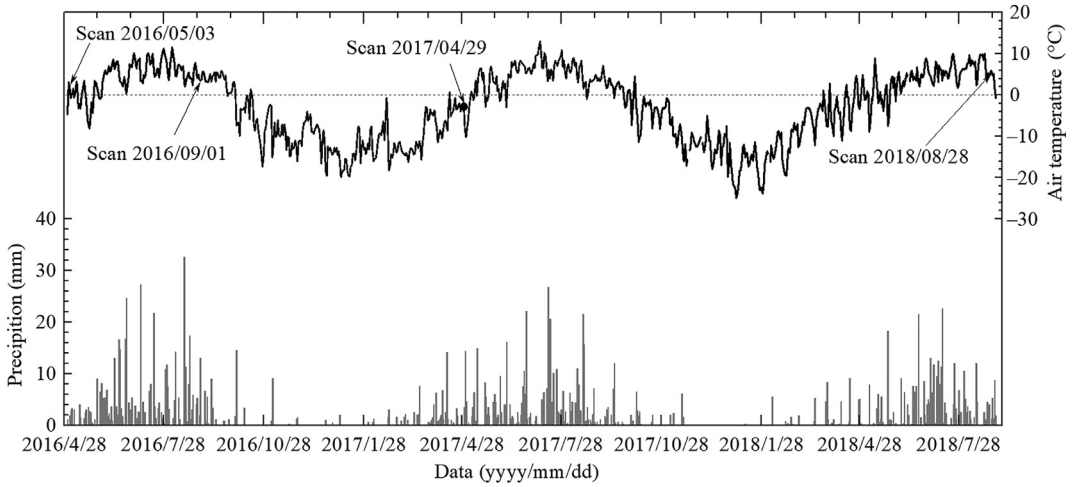

Fig. 6. Air temperature and precipitation observed at Daxigou meteorological station during the study period (3 May 2016−28 August 2018).

the present glacier mass is in disequilibrium with the current climate (Kraaijenbrink et al., 2017; Marzeion et al., 2018). As we know, changes in glacier geometry have a delayed response time to mass balance disturbance caused by climatic variation (Haeberli, 1995). Here we got glacier area changes to investigate the possible response time. The hanging glacier had an area of 0.053 km^2 and 0.051 km^2 in 2016 and 2018, respectively, with a shrinkage rate of 0.001 km^2 per year or 1.89% per year, which was large than the corresponding value of Urumqi Glacier (0.21% per year over two consecutive mass-balance years (2015−2017) (Xu et al., 2019) and mean value of 0.38% per year in the Chinese Tien Shan (Xing et al., 2017). Indicating hanging glaciers exhibited more rapid shrinkage compared with other morphological shapes of glaciers. If the glacier holds the current decrease rate, it will completely disappear within the next 50 years, which is shorter than the numerical simulation results of Urumqi Glacier No.1 (ultimately vanish within 50−90 years under different climate scenarios) (Li et al., 2021). The response of glaciers to climate change is complex and the delayed response time relies on glacier topographic and physical properties. Here we roughly estimated the response time based on the simple formula:

$$t_r = \overline{H}/\dot{a}_0 \tag{4}$$

where $\overline{H}$ equals the mean thickness of a glacier and $\dot{a}_0$ denotes the ablation rate at the glacier terminus (Cuffey and Paterson, 2010). The mean thickness of hanging glacier is generally less than similarly sized other morphological shapes of glaciers and we estimated the value according to statistical volume−area scaling proposed by Shi (2008) since the lack of *in-situ*-measured data:

$$\overline{H} = 34.4\, S^{0.45} \tag{5}$$

The calculated mean thickness was 9.01 m. Thus, we estimated the response time to be about 6−9 years ($\dot{a}_0$ was

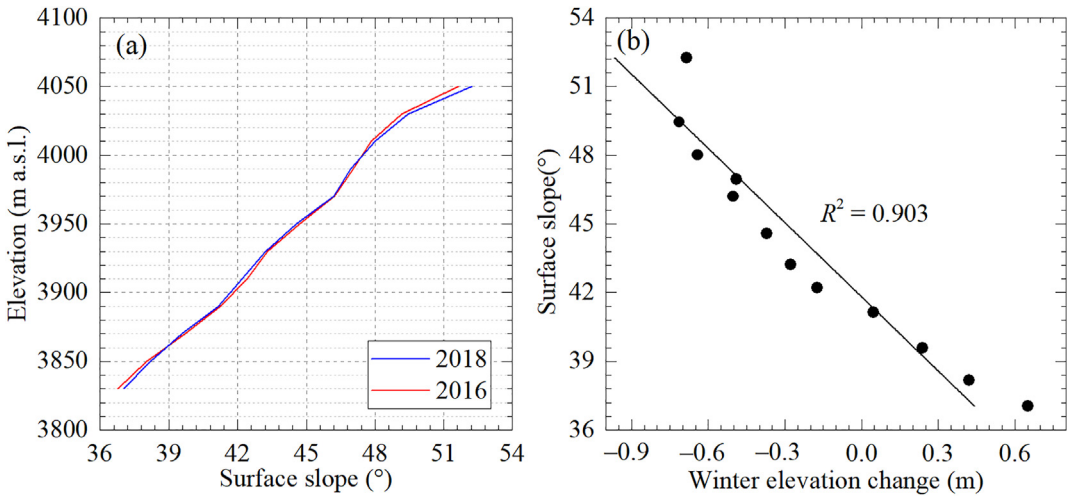

Fig. 7. (a) Hypsometry of glacier surface slope at the end of ablation season of 2016 and 2018 (in 10 m elevation bands), (b) relation between the surface slope and winter surface elevation changes.

Please cite this article as: XU, C.-H., et al., Rapid mass loss and disappearance of summer-accumulation type hanging glacier, Advances in Climate Change Research, https://doi.org/10.1016/j.accre.2021.11.001

1.0−1.5 m per year based on the repeated TLS surveys), which was far less than the response time of Urumqi Glacier No.1 (Wang et al., 2016). Note that the rough estimate was implemented by assuming that glacier mass balance perturbation remains constant. Therefore, the response time was probably rather shorter than the estimated value, suggesting that hanging glacier is very sensitive to climate warming and will experience rapid wastage and disappearance in future even climate change mitigation.

6. Conclusions

Here, we took a mid-latitude hanging glacier in the Tien Shan as a case and present the spatiotemporal pattern of seasonal and annual mass changes of the glacier according to the latest repeated TLS surveys. We discussed the possible mechanism of glacier changing behavior and its response to climate warming.

Our results indicated a high spatiotemporal variability of the distributed glacier surface elevation changes. Summer and annual elevation changes exhibited a common changing pattern, i.e., pronounced thinning occurred in the lower-elevation areas and weak thinning to slight thickening in higher-elevation parts, but winter elevation changing patterns were contrary, potentially due to the removal of existing snow depositions from the high elevations to glacier terminus. Resulting summer and annual mass balance were clearly negative (-1.38 ± 0.16 m w.e. and -0.86 ± 0.10 m w.e. per year for summer 2016 and the period 2016−2018, respectively), and the winter mass balance was nearly balanced (-0.10 ± 0.15 m w.e.), which may be attributed to very low air temperature and very poor precipitation. Compared with the adjacent Urumqi Glacier No. 1, altitudinal surface elevation lowering of the hanging glacier was generally larger, and the hanging glacier also exhibited more negative summer and annual mass balances, but the winter mass balance was more negative. The hanging glacier exhibited more rapid mass loss and the estimated response time of glaciers to climate change was very short (6−9 years), indicating hanging glaciers will experience rapid wastage and disappearance in the future even climate change mitigation. However, the present study is preliminary and our speculations about disappearance of the hanging glacier are mainly concluded from statistical and empirical formulas and we need more *in-situ*-measured data and numerical simulations to validate those speculations.

Declaration of competing interest

The authors declare no conflicts of interest.

Acknowledgments

This research was supported by the National Natural Science Foundation of China (42001067), the Natural Science Foundation of Gansu Province (21JR7RA059), the National Cryosphere Desert Data Center (20D03), the State Key Laboratory of Cryospheric Science (SKLCS-ZZ-2021), the Second Tibetan Plateau Scientific Expedition and Research (STEP) program (2019QZKK0201), and the National Natural Science Foundation of China (41771077).

References

Abermann, J., Fischer, A., Lambrecht, A., et al., 2010. On the potential of very high-resolution repeat DEMs in glacial and periglacial environments. Cryosphere 4, 53−65. https://doi.org/10.5194/tc-4-53-2010.

Colucci, R.R., Forte, E., Boccali, C., et al., 2015. Evaluation of internal structure, volume and mass of glacial bodies by integrated LiDAR and ground penetrating radar surveys: the case study of Canin Eastern Glacier (Julian Alps, Italy). Surv. Geophys. 36, 231−252. https://doi.org/10.1007/s10712-014-9311-1.

Cuffey, K.M., Paterson, W.S.B., 2010. The Physics of Glaciers, fourth ed. Butterworth-Heinemann, Oxford.

Faillettaz, J., Funk, M., Vagliasindi, M., 2016. Time forecast of a break-off event from a hanging glacier. Cryosphere 10, 1191−1200. https://doi.org/10.5194/tc-10-1191-2016.

Fischer, M., Huss, M., Kummert, M., et al., 2016. Application and validation of long-range terrestrial laser scanning to monitor the mass balance of very small glaciers in the Swiss Alps. Cryosphere 10, 1279−1295. https://doi.org/10.5194/tc-10-1279-2016.

Fugazza, D., Scaioni, M., Corti, M., et al., 2018. Combination of UAV and terrestrial photogrammetry to assess rapid glacier evolution and map glacier hazards. Nat. Hazards Earth Syst. Sci. 18, 1055−1071. https://doi.org/10.5194/nhess-18-1055-2018.

Gabbud, C., Micheletti, N., Lane, S.N., 2015. Lidar measurement of surface melt for a temperate Alpine glacier at the seasonal and hourly scales. J. Glaciol. 61 (229), 963−974. https://doi.org/10.3189/2015JoG14J226.

Haeberli, W., 1995. Glacier fluctuations and climate change detection. Geogr. Fis. Din. Quaternaria 18, 191−199.

Helfricht, K., Kuhn, M., Keuschnig, M., et al., 2014. Lidar snow cover studies on glaciers in the Ötztal Alps (Austria): comparison with snow depths calculated from GPR measurements. Cryosphere 8, 41−57. https://doi.org/10.5194/tc-8-41-2014.

Hoelzle, M., Azisov, E., Barandun, M., et al., 2017. Re-establishing glacier monitoring in Kyrgyzstan and Uzbekistan, Central Asia. Geosci. Instrum. Method. Data Syst. 6, 397−418. https://doi.org/10.5194/gi-6-397-2017.

Huss, M., 2013. Density assumptions for converting geodetic glacier volume change to mass change. Cryosphere 7, 877−887. https://doi.org/10.5194/tc-7-877-2013.

Huss, M., Bauder, A., Linsbauer, A., et al., 2021. More than a century of direct glacier mass-balance observations on Claridenfirn, Switzerland. J. Glaciol. 67 (264), 697−713. https://doi.org/10.1017/jog.2021.22.

Immerzeel, W.W., Kraaijenbrink, P.D.A., Shea, J.M., et al., 2014. High-resolution monitoring of Himalayan glacier dynamics using unmanned aerial vehicles. Remote Sens. Environ. 150, 93−103. https://doi.org/10.1016/j.rse.2014.04.025.

Joerg, P., Morsdorf, F., Zemp, M., 2012. Uncertainty assessment of multi-temporal airborne laser scanning data: a case study on an Alpine glacier. Remote Sens. Environ. 127, 118−129. https://doi.org/10.1016/j.rse.2012.08.012.

Klug, C., Bollmann, E., Galos, S.P., et al., 2018. Geodetic reanalysis of annual glaciological mass balances (2001−2011) of Hintereisferner, Austria. Cryosphere 12, 833−849. https://doi.org/10.5194/tc-12-833-2018.

Kraaijenbrink, P.D., Bierkens, M.F.P., Lutz, A.F., et al., 2017. Impact of a global temperature rise of 1.5 degrees Celsius on Asia's glaciers. Nature 549, 257−260. https://doi.org/10.1038/nature23878.

Li, Z., Li, H., Chen, Y., 2011. Mechanisms and simulation of accelerated shrinkage of continental glaciers: a case study of Urumqi Glacier No. 1 in Eastern Tianshan, central Asia. J. Earth Sci. 22 (4), 423−430. https://doi.org/10.1007/s12583-011-0194-5.

Li, Z., Li, H., Xu, C., et al., 2021. 60-year changes and mechanisms of Urumqi Glacier No. 1 in the eastern Tianshan of China, central Asia. Sci. Cold Arid Reg. 12 (6), 380−388. https://doi.org/10.3724/SP.J.1226.2020.00380.

Liu, C., Xie, Z., Wang, C., 1997. A research on the mass balance process of Glacier No.1 at the headwaters of the Urumqi River, Tianshan Mountains. J. Glaciol. Geocryol. 19 (1), 17−24 (Chinese).

López-Moreno, J.I., Revuelto, J., Rico, I., et al., 2016. Thinning of the Monte perdido glacier in the Spanish pyrenees since 1981. Cryosphere 10, 681−694. https://doi.org/10.5194/tc-10-681-2016.

Margreth, S., Funk, M., Tobler, D., et al., 2017. Analysis of the hazard caused by ice avalanches from the hanging glacier on the Eiger west face. Cold Reg. Sci. Technol. 144, 63−72. https://doi.org/10.1016/j.coldregions.2017.05.012.

Marzeion, B., Kaser, G., Maussion, F., et al., 2018. Limited influence of climate change mitigation on short-term glacier mass loss. Nat. Clim. Change 8, 305−308. https://doi.org/10.1038/s41558-018-0093-1.

Paul, F., 2008. Calculation of glacier elevation changes with SRTM: is there an elevation-dependent bias? J. Glaciol. 54, 945−946. https://doi.org/10.3189/002214308787779960.

Qin, D., 2016. Glossary of Cryospheric Science. China Meteorological Press, Beijing (Chinese).

RIEGL, 2014. 3D Terrestrial Laser Scanner Riegl VZ®-4000/Riegl VZ®-6000 General Description and Data Interfaces. RIEGL Laser Measurement Systems, Horn, Austria.

Rolstad, C., Haug, T., Denby, B., 2009. Spatially integrated geodetic glacier mass balance and its uncertainty based on geostatistical analysis: application to the western Svartisen ice cap, Norway. J. Glaciol. 55, 666−680. https://doi.org/10.3189/002214309789470950.

Schumann, G.J., Bates, P.D., 2018. The need for a high-accuracy, open-access global DEM. Front. Earth Sci. 6, 225. https://doi.org/10.3389/feart.2018.00225.

Shi, Y., 2008. Concise China Glacier Inventory. Shanghai Science Popularization Press, Shanghai (Chinese).

Ulrich, V., Williams, J.G., Zahs, V., et al., 2021. Measurement of rock glacier surface change over different timescales using terrestrial laser scanning point clouds. Earth Surf. Dyn. 9 (1), 19−28. https://doi.org/10.5194/esurf-9-19-2021.

Vincent, C., Thibert, E., Harter, M., et al., 2015. Volume and frequency of ice avalanches from Taconnaz hanging glacier, French Alps. Ann. Glaciol. 56 (70), 17−25. https://doi.org/10.3189/2015AoG70A017.

Wang, P., Li, Z., Li, H., et al., 2014. Comparison of glaciological and geodetic mass balance at Urumqi Glacier No. 1, Tian Shan, central Asia. Global Planet. Change 114, 14−22. https://doi.org/10.1016/j.gloplacha.2014.01.001.

Wang, P., Li, Z., Li, H., et al., 2016. Analyses of recent observations of Urumqi Glacier No. 1, Chinese Tianshan mountains. Environ. Earth Sci. 75, 720. https://doi.org/10.1007/s12665-016-5551-3.

WGMS (World Glacier Monitoring Service), 2020. Global Glacier Change Bulletin No. 3 (2016−2017) Zurich. https://doi.org/10.5904/wgms-fog-2019-12.

Xing, W., Li, Z., Zhang, H., et al., 2017. Spatial-temporal variation of glacier resources in Chinese Tianshan Mountains since 1959. Acta Geograph. Sin. 72 (9), 1594−1605 (Chinese).

Xu, C., Li, Z., Wang, P., et al., 2018a. Detailed comparison of glaciological and geodetic mass balances for Urumqi Glacier No. 1, eastern Tien Shan, China, from 1981 to 2015. Cold Reg. Sci. Technol. 155, 137−148. https://doi.org/10.1016/j.coldregions.2018.08.006.

Xu, C., Li, Z., Li, H., et al., 2019. Long-range terrestrial laser scanning measurements of annual and intra-annual mass balances for Urumqi Glacier No. 1, eastern Tien Shan, China. Cryosphere 13, 2361−2383. https://doi.org/10.5194/tc-13-2361-2019.

Xu, M., Kang, S., Wu, H., et al., 2018b. Detection of spatio-temporal variability of air temperature and precipitation based on long-term meteorological station observations over Tianshan Mountains, Central Asia. Atmos. Res. 203, 141−163. https://doi.org/10.1016/j.atmosres.2017.12.007.

Yang, D., Kang, E., Felix, B., 1992. Characteristics of precipitation in the source area of the Urumqi River basin. J. Glaciol. Geocryol. 14 (3), 258−266 (Chinese).

Yue, X., Zhao, J., Li, Z., et al., 2017. Spatial and temporal variations of the surface albedo and other factors influencing Urumqi Glacier No. 1 in Tien Shan, China. J. Glaciol. 63 (241), 899−911. https://doi.org/10.1017/jog.2017.57.

Zemp, M., Frey, H., Gärtner-Roer, I., et al., 2015. Historically unprecedented global glacier decline in the early 21st century. J. Glaciol. 61 (228), 745−762. https://doi.org/10.3189/2015JoG15J017.

Zemp, M., Huss, M., Thibert, E., et al., 2019. Global glacier mass changes and their contributions to sea-level rise from 1961 to 2016. Nature 568, 382−386. https://doi.org/10.1038/s41586-019-1071-0.

Please cite this article as: XU, C.-H., et al., Rapid mass loss and disappearance of summer-accumulation type hanging glacier, Advances in Climate Change Research, https://doi.org/10.1016/j.accre.2021.11.001